2015

Distance-dependent plasmon-enhanced fluorescence of upconversion nanoparticles using polyelectrolyte multilayers as tunable spacers

Ai Ling Feng
Xi'an Jiaotong University

Min Li You
Xi'an Jiaotong University

Limei Tian
Washington University School of Medicine in St. Louis

Srikanth Singamaneni
Washington University School of Medicine in St. Louis

Ming Liu
Xi'an Jiaotong University

See next page for additional authors

SCIENTIFIC REPORTS

OPEN

SUBJECT AREAS:
NANOPHOTONICS AND PLASMONICS
NANOPARTICLES

Received
3 October 2014

Accepted
10 December 2014

Published
14 January 2015

Correspondence and requests for materials should be addressed to M.L. (minlin@mail.xjtu.edu.cn)

Distance-Dependent Plasmon-Enhanced Fluorescence of Upconversion Nanoparticles using Polyelectrolyte Multilayers as Tunable Spacers

Ai Ling Feng[1,2], Min Li You[1,2], Limei Tian[3], Srikanth Singamaneni[3], Ming Liu[4], Zhenfeng Duan[5], Tian Jian Lu[2], Feng Xu[1,2] & Min Lin[1,2,5]

[1]The Key Laboratory of Biomedical Information Engineering, Ministry of Education, School of Life Science and Technology, Xi'an Jiaotong University, Xi'an 710049, P.R. China, [2]Bioinspired Engineering and Biomechanics Center (BEBC), Xi'an Jiaotong University, Xi'an 710049, P.R. China, [3]Department of Mechanical Engineering and Materials Science, Institute of Materials Science and Engineering, Washington University in St. Louis, St Louis, MO 63130, USA, [4]Electronic Materials Research Laboratory, Key Laboratory of the Ministry of Education & International Center for Dielectric Research, Xi'an Jiaotong University, Xi'an 710049, P.R. China, [5]Center for Sarcoma and Connective Tissue Oncology, Massachusetts General Hospital, Harvard Medical School, MA 02114, USA.

Lanthanide-doped upconversion nanoparticles (UCNPs) have attracted widespread interests in bioapplications due to their unique optical properties by converting near infrared excitation to visible emission. However, relatively low quantum yield prompts a need for developing methods for fluorescence enhancement. Plasmon nanostructures are known to efficiently enhance fluorescence of the surrounding fluorophores by acting as nanoantennae to focus electric field into nano-volume. Here, we reported a novel plasmon-enhanced fluorescence system in which the distance between UCNPs and nanoantennae (gold nanorods, AuNRs) was precisely tuned by using layer-by-layer assembled polyelectrolyte multilayers as spacers. By modulating the aspect ratio of AuNRs, localized surface plasmon resonance (LSPR) wavelength at 980 nm was obtained, matching the native excitation of UCNPs resulting in maximum enhancement of 22.6-fold with 8 nm spacer thickness. These findings provide a unique platform for exploring hybrid nanostructures composed of UCNPs and plasmonic nanostructures in bioimaging applications.

Fluorescence imaging by using nanoparticles as probes is a powerful non-invasive modality with high sensitivity and amenability to targeting for bioimaging and biolabeling[1–4]. As next generation fluorescence probe candidates, UCNPs emitting visible light when excited by near-infrared light have been extensively investigated[5–7]. Compared with organic fluorophores and quantum dots, UCNPs exhibit unique optical and physical properties, such as significantly reduced background autofluorescence, photobleaching, DNA photodamage to biological specimens and phototoxicity[8–10]. However, the quantum yield of UCNPs is relatively low (<1%) due to the small absorption cross-sections (the ability to absorb a photon of a specific wavelength and polarization)[11,12]. In addition, compared with their bulk counterparts, the dopant ion concentration on the surface of UCNPs is relatively high and is expected to be quenched by surface quenchers[13]. The above-mentioned reasons will result in reduced fluorescence intensity of UCNPs, limiting their application in fluorescence imaging especially in deep tissue imaging. Therefore, enhancing fluorescence intensity of UCNPs is significantly critical and necessary.

Recently, various methods have been explored to enhance the fluorescence intensity of UCNPs, such as tuning the types and concentrations of lanthanide-doped ions[14,15], modulating the morphology of nanoparticles[16], increasing the diameter of nanoparticles[17], coating the inert shell onto the surface of UCNPs[18–20] and using plasmon nanoantenna architecture[21–26]. Among these methods, plasmon-enhanced fluorescence strategy has attracted considerable attention. The mechanism of plasmon enhancement can be mainly attributed to the increased excitation rate due to a local field enhancement effect and the increased emission rate by surface plasmon coupled emission, which can enhance both the quantum yield and fluorescence intensity[16,27].

The LSPR coupled fluorescence enhancement is a complex process affected by a variety of parameters including sizes and morphologies of the metal and fluorescent nanoparticles, particle concentration, interparticle distance and spectra relationship of the fluorescence materials and metal nanoparticles[28–30]. Among these parameters, distance and spectra characteristics (*i.e.*, absorption and emission of the fluorescence materials and LSPR wavelength of the plasmon nanostructures) play important roles in enhancing fluorescence intensity. Previous studies on the effect of distance between UCNPs and plasmon nanostructure on fluorescence enhancement were performed either by using SiO_2[31], TiO_2[32] and Al_2O_3[33] as spacers or using the tip from atomic force microscopy (AFM) for distance modulation[24]. However, it is difficult to precisely modulate the distance with high resolution by using SiO_2, TiO_2 and Al_2O_3 as spacers. As for AFM modulation, the complex operating process and expensive equipment are needed which prohibited its widespread applications. The spectra dependence of plasmon enhancement for UCNPs was studied by using gold nanohole arrays[34] or Ag nano-film with ultra-broad plasmon resonance band as plasmon nanoantenna[35]. These methods either involve sophisticated fabrication process or are difficult to systematically tune LSPR wavelength absorption of metal nanostructure. In addition, enhancement factors reported in the literature are highly inconsistent and the mechanism underlying plasmon enhancement is still not clear. Therefore, there is an urgent need to establish a simple and effective method to study the influence of the distance and spectra properties on fluorescence enhancement in a reliable and precise manner.

In this article, we developed a novel plasmon-enhanced fluorescence system comprised of UCNPs and AuNRs using a simple and reproducible immersion-based method by layer-by-layer self-assembly process. Polyelectrolyte multilayers were used as spacers to precisely control the distance between UCNPs and AuNRs with a spatial resolution of nm-precision. AuNRs were chosen as plasmon nanoantennae considering the facile tunability of their longitudinal LSPR wavelength by changing the aspect ratio of nanostructures. We experimentally and theoretically demonstrated a significant dependence of upconversion fluorescence enhancement on the distance between UCNPs and AuNRs. Furthermore, we used AuNRs with three different LSPR wavelengths to investigate the influence of the spectra properties of the nanostructures on the upconversion fluorescence intensity. It was observed that the plasmon-enhanced fluorescence had a strong spectra dependence, with a significant enhancement when the LSPR wavelength of the AuNRs almost overlapped with the native excitation of UCNPs (980 nm). This work represents a systematic investigation of plasmon-enhanced upconversion luminescence and lays the groundwork for a novel class of hybrid nanoprobes for bioimaging and detection applications.

Results

Synthesis strategy of a novel UCNPs and AuNRs plasmon-enhanced fluorescence system. To obtain ultrabright fluorescence bullets for bioimaging and biolabeling, a novel UCNPs and AuNRs plasmon-enhanced fluorescence system was conveniently fabricated without need for any expensive equipment or complicated procedures (Fig. 1a). In this paper, polyelectrolyte multilayers composed of positively charged poly allylamine hydrochloride (PAH) and negatively charged sodium polystyrene sulfonate (PSS) were used as spacers by the immersion-based layer-by-layer self-assembly procedure based on electrostatic interactions. The assembly method provides accurate control over the thickness of dielectric spacer on the nanometer scale. Plasmon-enhanced fluorescence was investigated by changing the thickness of polyelectrolyte layers to precisely modulating the distance between UCNPs and AuNRs as plasmon nanostructures (Fig. 1b). And for the extraordinary AuNRs/Polyelectrolytes/UCNPs trilayer structures, spectra-dependence behavior of plasmon-enhanced fluorescence was achieved by using AuNRs with different aspect ratios of 7.6, 6.3 and 4.5 (named AuNRs-980, AuNRs-915 and AuNRs-735, Supplementary Table S1) (Fig. 1c).

Preparation and characterization of nanoparticles. The $NaYF_4$:Yb,Er nanoparticles were synthesized via a thermal decomposition procedure in an oleic acid and oleylamine system. Representative transmission

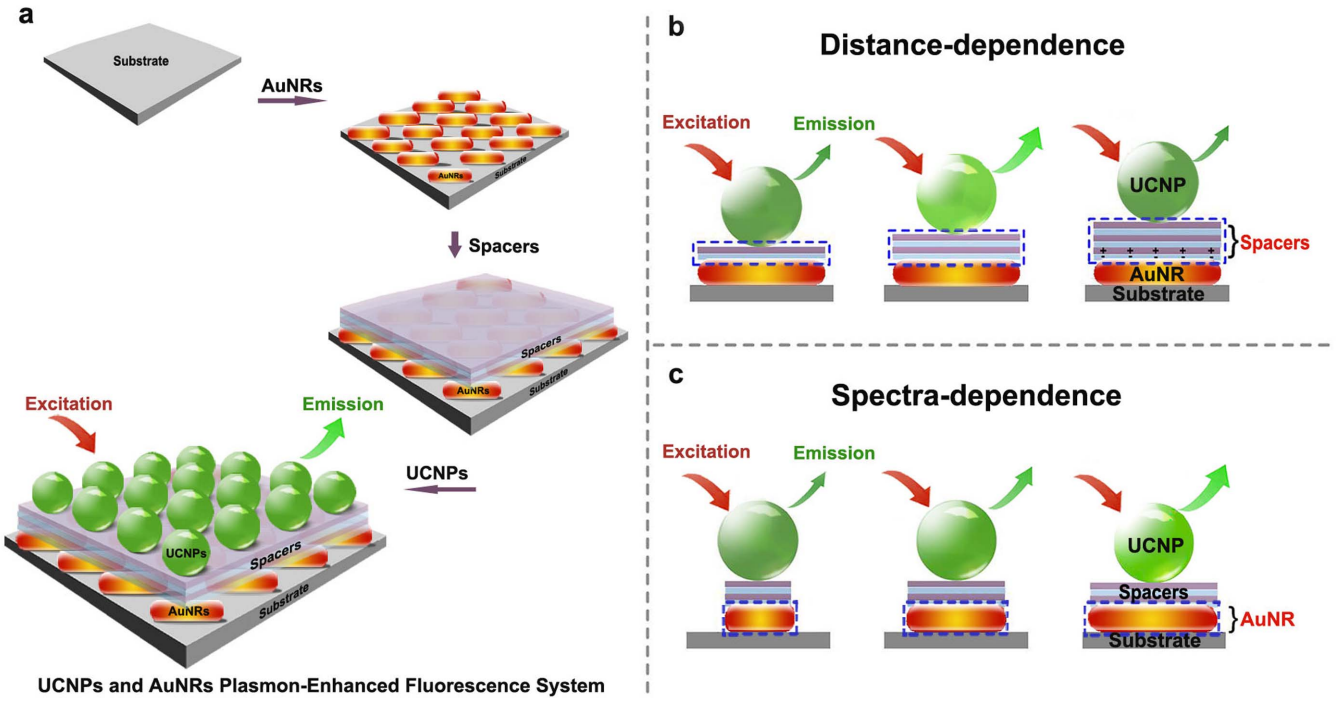

Figure 1 | Synthesis strategy and mechanism study of UCNPs and AuNRs plasmon-enhanced fluorescence system. (a) Fabrication process of a novel UCNPs and AuNRs plasmon-enhanced fluorescence system. (b) Distance dependent and (c) Spectra dependent plasmon-enhanced fluorescence of UCNPs. Distance-dependent plasmon-enhanced fluorescence was investigated by fine-tuning the spacer thickness via layer-by-layer self-assembly of polyelectrolyte multilayers. Spectra-dependent plasmon-enhanced fluorescence was achieved by using different aspect ratios of AuNRs.

electron microscopy (TEM) micrograph of the as-synthesized $NaYF_4$:Yb,Er nanoparticles is shown in Fig. 2a. The UCNPs are hexagonal in shape and nearly monodispersed in size (average size 38.7 nm, standard deviation 1.9 nm, Supplementary Fig. S1). The high resolution transmission electron microscopy (HRTEM) image of UCNPs shows the adjacent lattice fringes distance of 0.515 nm, which can be assigned to the (100) crystal plane of the hexagonal-phased $NaYF_4$[36] (the inset graph of Fig. 2a). The diffraction pattern of $NaYF_4$:Yb,Er nanoparticles in Fig. 2b shows three bright rings corresponding to the interplanar spacing (d-values) of hexagonal phase. The X-ray diffraction (XRD) patterns of UCNPs provide further evidence for the formation of pure hexagonal phase $NaYF_4$ (JCPDS files No.16-0334), Fig. 2c. The as-prepared $NaYF_4$:Yb,Er nanoparticles are hydrophobic due to the capped oleic acid from the organic solvent as ligand on their surface.

To make the as-prepared nanoparticles water-soluble, a uniform polyacrylic acid (PAA) layer was coated on their surface. We observed no significant change in the UCNPs morphology after the surface modification with PAA coating (Supplementary Fig. S2). The capping functional groups on the surface of UCNPs with PAA coating were confirmed by Fourier-transform infrared spectroscopy (FT-IR), Fig. 2d. UCNPs-PAA exhibits a broad band at around 3336 cm^{-1}, which is conformed with the O-H stretching vibration. The bands at 2917 and 2849 cm^{-1} in the FT-IR spectrum can be separately assigned to the asymmetric and symmetric stretching vibrations of the $-CH_2$ in the alkyl chain. The strong transmission band at 1731 cm^{-1} indicates the existence of the -COOH on the surface of UCNPs-PAA[37]. These results confirmed the coating of PAA on the surface of UCNPs. Upconversion fluorescence photos (left) and bright-field (right) of UCNPs dissolved in cyclohexane and UCNPs-PAA dissolved in water (the concentration of UCNPs and UCNPs-PAA is 15 $mg \cdot mL^{-1}$) are shown in Fig. 2e, f. Both UCNPs and UCNPs-PAA show strong green emission when excited by 980 nm laser (Fig. 2e, f, left). The as-prepared $NaYF_4$:Yb,Er nanoparticles are soluble in cyclohexane (Fig. 2e, right). After PAA coating, the nanoparticles become water-soluble with good chemical stability (Fig. 2f, right), which is very important for the following experiment. After PAA modification, the surface charge of UCNPs is altered with zeta potential varying from -28 to -46 mV (Fig. 2g), confirming that the -COOH groups have been successfully grafted onto UCNPs. The existence of -COOH groups on their surfaces results in high water solubility and improves zeta potential. Meanwhile, AuNRs-980, AuNRs-915 and AuNRs-735 with different aspect ratios are positively-charged with zeta potential of +48.1 mV, +49.7 mV and +30.8 mV, as seen in Fig. 2g. The strong charge of AuNRs provides an effective way of electrostatic interactions for the following layer-by-layer (LbL) self-assembly process.

Distance-dependent plasmon-enhanced fluorescence analysis of upconversion nanoparticles. To measure the thickness of polyelectrolyte multilayers, AFM was performed at the edge of an intentional scratch (scratch test) (Fig. 3a, b). The AFM height profile shows that thickness is about 8 nm after deposition of four bilayers of polyelectrolyte (Fig. 3b), indicating a thickness of ~2 nm for each bilayer, which is in agreement with our previous reports[38]. The uniform distribution of AuNRs and UCNPs on silicon slides is confirmed by scanning electron microscopy (SEM) image (Fig. 3c, d). The average area density of AuNRs and UCNPs is 74 μm^{-2} and 217 μm^{-2}, respectively.

To study the influence of distance on fluorescence intensity, we used AuNRs-980 as plasmonic nanostructures due to the overlapping of its LSPR absorption band with the excitation wavelength of

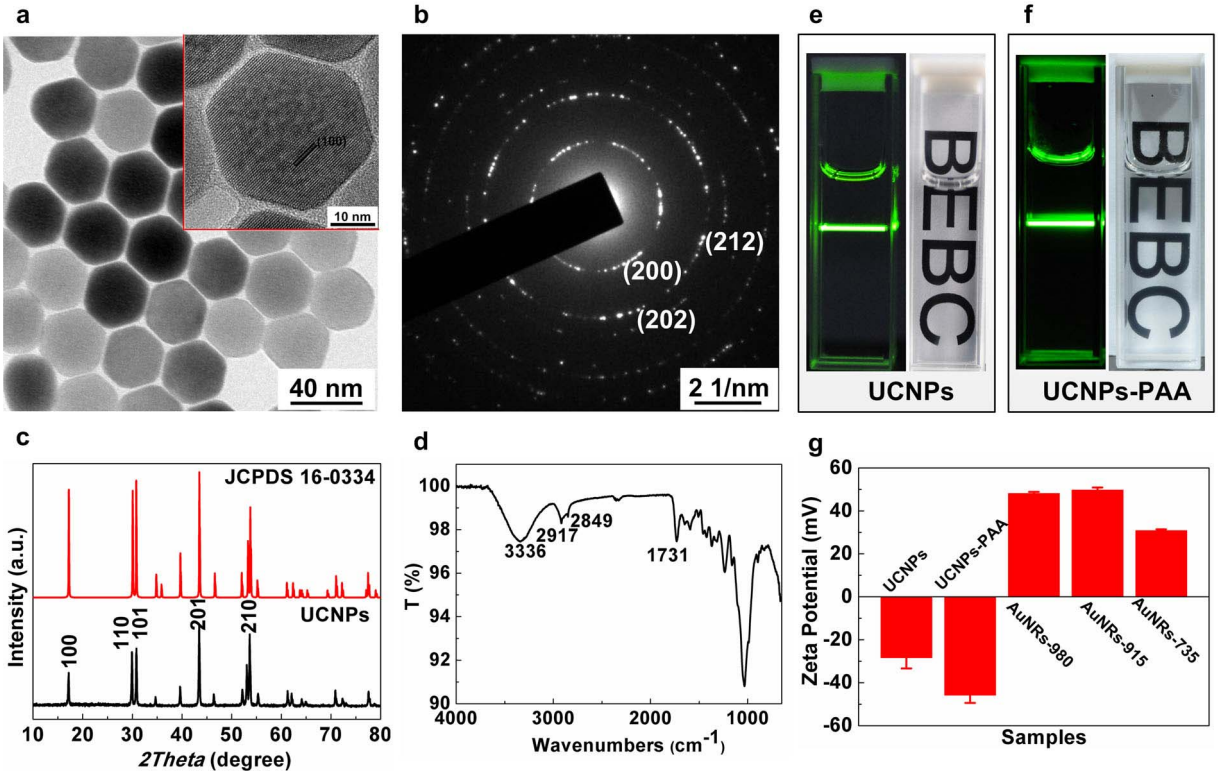

Figure 2 | Characterization of nanoparticles. (a) Representative TEM image of UCNPs, the inset showing HRTEM of UCNPs; (b) Diffraction pattern of UCNPs and (c) XRD pattern of UCNPs, indicating the formation of pure hexagonal phase $NaYF_4$; (d) FT-IR spectrum of UCNPs-PAA showing the existence of -COOH group; Upconversion fluorescence photos (left) and bright-field (right) of: (e) UCNPs dissolved in cyclohexane and (f) UCNPs-PAA dissolved in water (the concentration of UCNPs and UCNPs-PAA is 15 $mg \cdot mL^{-1}$); (g) Zeta potential of UCNPs, UCNPs-PAA and AuNRs with different aspect ratios.

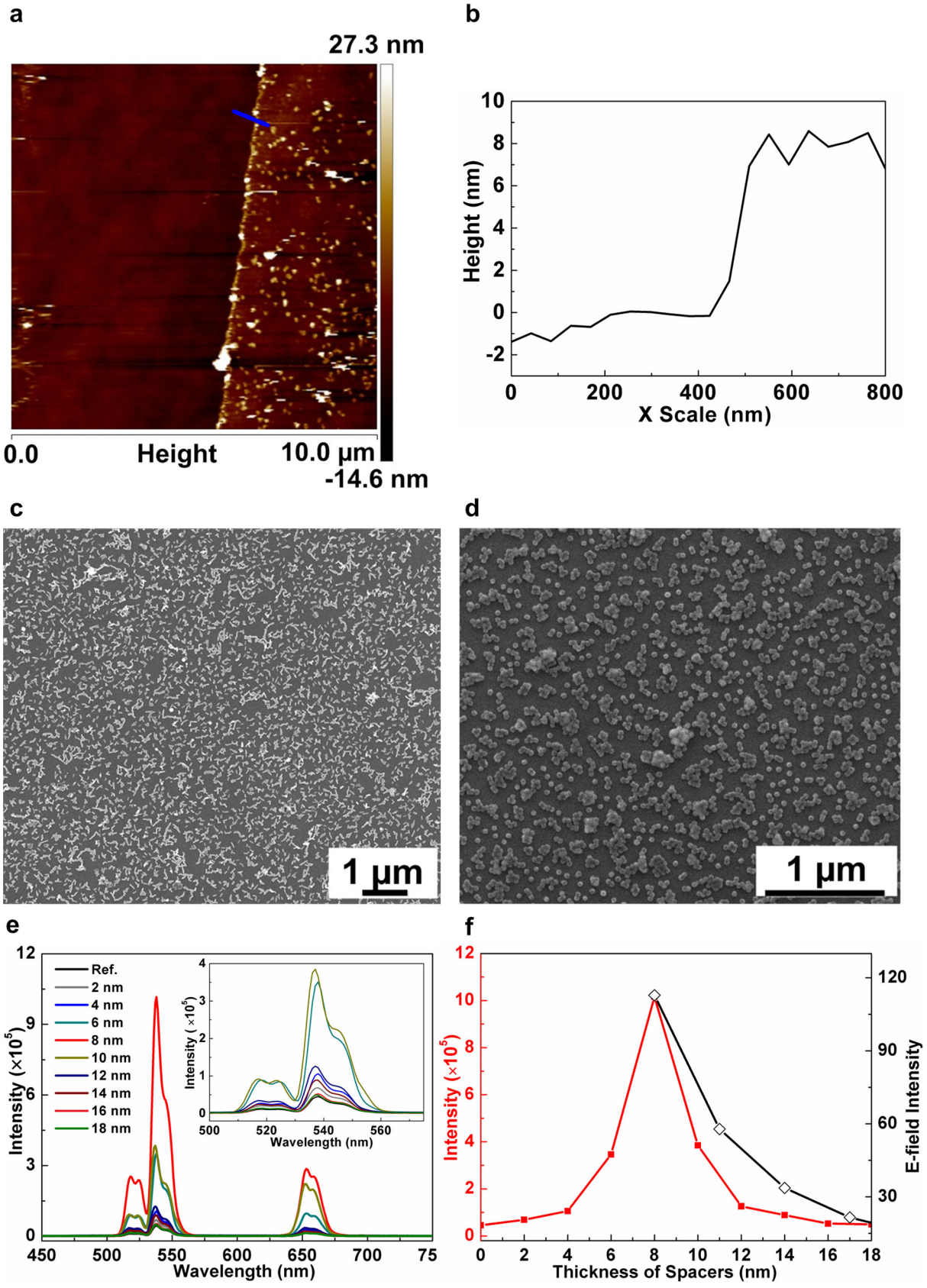

Figure 3 | **Distance-dependent plasmon-enhanced fluorescence analysis of UCNPs.** (a) AFM image of a scratched AuNRs-980 film on silicon substrate, showing the thickness of four polyelectrolyte bilayers; (b) Change in height along the probing path labelled with blue line in (a); SEM image of: (c) AuNRs on silicon substrate coated by PSS layer; (d) UCNPs on silicon substrate coated by one polyelectrolyte bilayers, indicating the uniform distribution and optimal density of AuNRs and UCNPs on silicon slides; (e) Fluorescence spectra of UCNPs separated from the surface of AuNRs by different thicknesses of polyelectrolyte layers (the inset showing the partial enlarged view); (f) Correlation of the distance from the AuNRs surface to the fluorescence intensity (red line) at 540 nm from (e) and electric field intensity (black line).

UCNPs (980 nm). Fluorescent spectra were collected under the excitation of a 980 nm continuous-wave laser (laser power of 250 mW). Distance-dependent plasmon-enhanced upconversion fluorescence was obtained by separating UCNPs at different distances from the AuNRs-980 using 2, 4, 6, 8, 10, 12, 14, 16 and 18 polyelectrolyte multilayers. The corresponding upconversion luminescence spectra for $NaYF_4$:Yb,Er nanoparticles with different distances are shown in Fig. 3e (the inset showing the partial enlarged view). There are two main characteristic emission bands including a strong green emission peaking at 540 nm corresponding to $^2H_{11/2}/^4S_{3/2}$-$^4I_{15/2}$ and the other weak red emission peaking at 650 nm corresponding to $^4F_{9/2}$-$^4I_{15/2}$. Energy level diagram illustrates the mechanism of $NaYF_4$:Yb,Er upconversion luminescence with the 980 nm laser excitation (seen in Supplementary Fig. S3)[21]. The fluorescence intensity at 540 nm as a function of thickness of polyelectrolyte spacers was plotted on Fig. 3f. As the thickness of spacers increases, plasmon-induced luminescence enhancement of UCNPs is observed. The fluorescence intensity reaches a maximum at the layer thickness of 8 nm, after which the fluorescence intensity decreases gradually back to that of the UCNPs without plasmon enhancement.

Here, we define the enhancement factor as I/I_0, where I and I_0 are the fluorescence intensities of UCNPs with and without plasmon enhancement. A maximum enhancement factor of about 22.6 is achieved at 540 nm emission peak with a spacer thickness of 8 nm. The results suggest that optimal distance between UCNPs and plasmon nanostructures was critical to obtain maximum fluorescence intensity. To further understand the relationship between the spacer thickness and the plasmon-enhanced luminescence intensity, we performed a finite difference time-domain (FDTD) simulation. The simulation provides the electric field intensity near the surface of single AuNRs in air. The simulated electric field intensity decreases exponentially with increasing distance, corresponding to the decay in upconversion fluorescence intensity for spacer thickness of over 8 nm (Fig. 3f).

Localized surface plasmon resonance (LSPR) that arises due to collective oscillation of electrons of the noble metal nanoparticles can have either enhancement or quenching effects depending on the distance of UCNPs separated from the metal surface and the relative position of the LSPR wavelength from the excitation or emission wavelength of UCNPs[39]. That is to say, quantum efficiencies and luminescence intensity of UCNPs can be enhanced or quenched by their surrounding metal nanoparticles[40]. Plasmon enhancement of the upconversion luminescence could be attributed to three competing effects[25,31,41,42]: (1) an increased excitation rate induced by local field enhancement (LFE) causing enhanced excitation efficiency resulting in fluorescence enhancement; (2) an increased radiative decay rate by surface plasmon-coupled emission (SPCE) from coupling of the upconversion emission with the AuNRs LSPR wavelength, resulting in fluorescence enhancement; (3) the non-radiative energy transfer (NRET) from the UCNPs to the AuNRs resulting in fluorescence quenching. NRET process dominates at the surface and drops off with inverse fourth power of localized electric field[41]. While LFE effect drops off exponentially from the surface[41]. There is an equilibrium between NRET and LFE effects that affects the plasmon enhancement extent. The effect (1) takes its power by increasing the excitation rate in the vicinity of UCNPs which is dependent on many parameters including the dielectric permittivity of the metal, the nanoparticle size, and the intrinsic quantum yield of UCNPs, especially the distance and excitation wavelength[43,44]. The effects (2, 3) arise from variation of the radiative and non-radiative processes of upconversion luminescence via near-field interaction between UCNPs and metal nanoparticles[44]. These effects result in either facilitating radiation to the far field (i.e. emission luminescence) or the energy transfer process of UCNPs to the metal surface[45]. The NRET process between UCNPs and metal nanoparticles can enhance non-radiative decay rate and reduce the quantum yield of UCNPs, resulting in the reduced luminescence intensity[42]. NRET depends mainly on distance between UCNPs and metal nanoparticles and is independent of the excitation wavelength[25]. Therefore, when UCNPs are in very close proximity with AuNRs-980 surface (for example ~2 nm), NRET dominates, which results in relatively weak fluorescence. As the distance increases, the LFE effect becomes significant, contributing to the enhancement of fluorescence intensity[46]. The emission intensity reaches maximum at an optimal distance of about 8 nm. The fluorescence intensity reduces gradually with further increase in distance, accompanying with gradually reduced electric field (Fig. 3f). When the distance is increased to ~18 nm, the fluorescence intensity of UCNPs enhanced by AuNRs is comparable to that of the bare UCNPs employed as reference. At such large distance from the surface of AuNRs, electric field intensity is insignificant, causing no observable enhancement of upconversion emission from UCNPs.

Spectra-dependent plasmon-enhanced fluorescence analysis of upconversion nanoparticles. In addition to the study of distance-dependent upconversion luminescence, we systematically investigated the influence of LSPR wavelength of AuNRs on upconversion luminescence (the relationship between LSPR wavelength of AuNRs and excitation wavelength of UCNPs). Representative TEM images of AuNRs with three different aspect ratios are shown in Fig. 4a–c. The average diameters of the AuNRs are about 14.1 ± 1.7, 14.0 ± 1.5 and 14.7 ± 1.8 nm, while the average lengths are about 105.5 ± 20.2, 86.6 ± 10.7 and 64.4 ± 7.3 nm, corresponding to aspect ratio of 7.6 ± 1.9, 6.3 ± 1.0 and 4.5 ± 0.8, respectively (Supplementary Fig. S4 and Supplementary Table S2). Meanwhile, the simulated results of electric field surrounding the surface of AuNRs are shown as inset graph in Fig. 4a–c. The LSPR wavelength red-shifts with increase in aspect ratio of AuNRs. The LSPR wavelength of the AuNRs with aspect ratio of 7.6, 6.3 and 4.5 measured in water is 1075, 1010, and 830 nm, respectively (Supplementary Fig. S5). The corresponding LSPR wavelengths of the AuNRs measured in air are 980, 915 and 735 nm (Fig. 4d). The significant blue shift (~95 nm, Supplementary Table S1) in the LSPR of AuNRs from water to air is due to the different effective refractive index of the medium around AuNRs[47].

In our experiments, the optimized dielectric spacer distance of 8 nm was employed for the preparation of samples. The fluorescence spectra of UCNPs and AuNRs plasmon-enhanced fluorescence system under 980 nm laser excitation are shown in Fig. 4e. We observed a significant dependence of plasmon-enhanced fluorescence intensity on the LSPR wavelength of the AuNRs. Compared with the reference (bare UCNPs), UCNPs plasmon-enhanced by AuNRs-980 and AuNRs-915 are found to have stronger fluorescence emission. Meanwhile, no significant enhancement of UCNPs emission is observed for AuNR-735 (Fig. 4f). The enhancement factors reach 22.6, 12.0 and 1.1 for UCNPs enhanced by AuNRs-980, AuNRs-915 and AuNRs-735 at 540 nm green emission, respectively (Fig. 4f). In the case of AuNRs-980, the maximum fluorescence emission is achieved. When the LSPR wavelength of the AuNRs-980 almost overlaps with the excitation of UCNPs (980 nm, Fig. 4d), the energy is efficiently collected by the AuNRs and transferred from the plasmon nanostructure to the electrons of UCNPs, which leads to an increase in the absorption cross-section of the UCNPs (Fig. 4d)[34]. Partial match of the LSPR wavelength of AuNRs-915 with the excitation of UCNPs (Fig. 4d) contributes to a 12.0-fold enhancement of fluorescence intensity as compared with the reference. In the case of AuNRs-735, the LSPR wavelength is far away from the excitation wavelength of UCNPs which leads to negligible fluorescence enhancement.

We simulated electric field intensity surrounding the three kinds of single AuNRs (Fig. 4f, black curve) by FDTD simulation. For AuNRs-980, AuNRs-915 and AuNRs-735, the electric field intensity

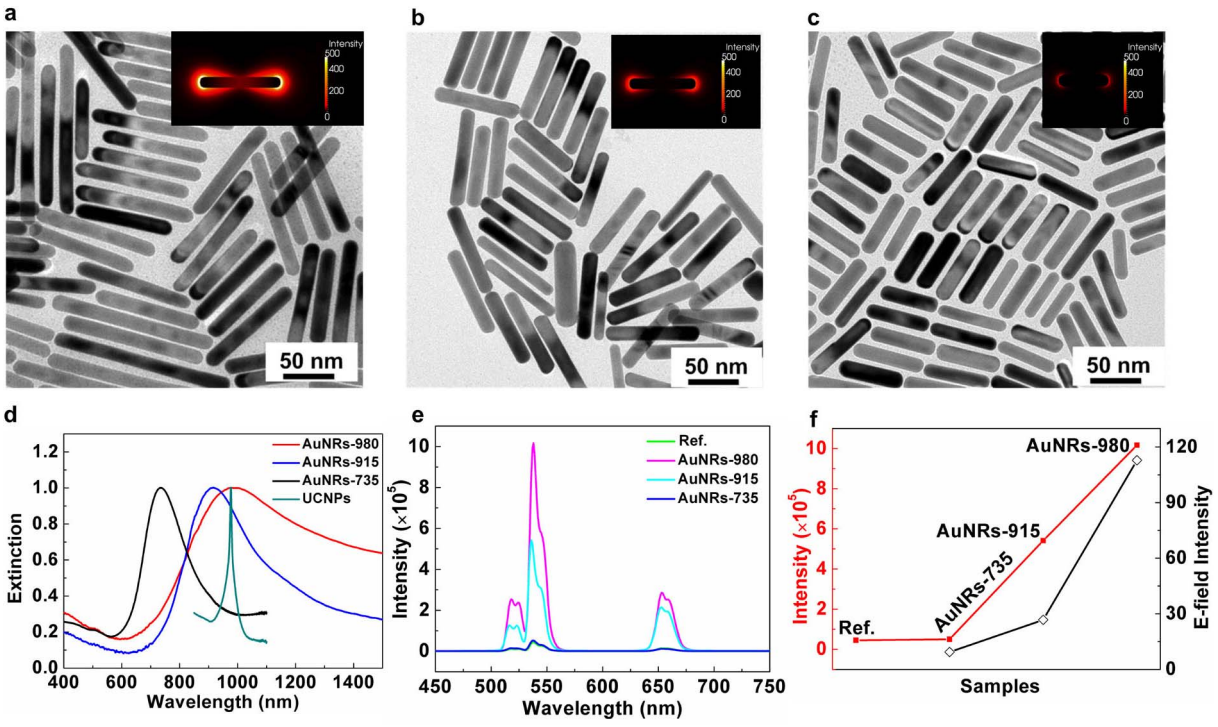

Figure 4 | Spectra-dependent plasmon-enhanced fluorescence analysis of UCNPs. TEM images of AuNRs with different aspect ratios: (a) 7.6 (AuNRs-980); (b) 6.3 (AuNRs-915); (c) 4.5 (AuNRs-735); the inset in (a–c) showing simulated electric field surrounding AuNRs. (d) UV-Vis-NIR extinction spectra of UCNPs, AuNRs-980, AuNRs-915 and AuNRs-735 on silicon substrate. The maximum overlap of extinction wavelength between the UCNPs and AuNRs-980 facilitates optimal plasmon fluorescence enhancement. (e) Fluorescence spectra of UCNPs deposited on AuNRs-980, AuNRs-915 and AuNRs-735 spaced by four polyelectrolyte bilayers with the distance of about 8 nm; (f) Correlation of different aspect ratios of the AuNRs to the fluorescence intensity (red line) and electric field intensity (black line).

reduced gradually, which is in good agreement with the experimental results of the fluorescence intensity, confirming the electric field coupling effect of AuNRs and UCNPs. In fact, multiple nanorods may alter the spectral characteristics of UCNPs. This could be attributed to the difference in the intensity of electric field between single and multiple AuNRs, whereas the change in electric field intensity will not alert the mechanism underline electric field enhanced luminescence intensity. In our experiments, the distribution of AuNRs on silicon slides is random (Fig. 3c), including side-by-side, head-to-head and even disorganized. The dielectric and cluster of AuNRs have great influence on electric field intensity, while not the electric field distribution. For example, we simulated two special arrangements of AuNRs on polymer surface: side-by-side and head-to-head. Our simulated results demonstrated that the distribution of electric field is similar to the individual AuNRs (Supplementary Fig. S6). Therefore, simulation of the electric field surrounding a single AuNR is able to reveal the distance dependent plasmonic enhancement process. To check the influence of dielectric layers, we simulated and compared the distribution of electric field surrounding AuNRs in air (Fig. 4a–c) and in polymer (Supplementary Fig. S7 and Supplementary Fig. S8). We found that the distribution of electric field was also similar when dielectric permittivity surrounding AuNRs was changed.

Fluorescence lifetime analysis. To further confirm the plasmon-enhanced effect on upconversion luminescence, we measured time-resolved upconversion fluorescence lifetimes under a 980 nm pulse laser excitation. The rise and decay time of the green emission at 540 nm from UCNPs enhanced by AuNRs-980 with spacer thickness of 8 nm (PEFS) and bare UCNPs (Ref.) are shown in Fig. 5a, b. Since the rise and decay time of the fluorescence cannot be fitted as mono-exponential, we determined the rise and decay time by half of its maximal value following literature[24,42]. Compared with UCNPs without plasmon enhancement effect (black curve in Fig. 5a), UCNPs with AuNRs-980 enhancement (red curve in Fig. 5a) revealed a significant decrease in the rise time from τ = 303.6 μs to τ = 220.5 μs. This decrease in rise time is consistent with plasmon enhancement, which originates from an increased excitation rate of Yb^{3+} due to the coupling of the LSPR absorption of wavelength AuNRs-980 and excitation of UCNPs[24,44]. The rate of energy transfer from Yb^{3+} to Er^{3+} ions also increases (seen the energy level scheme, Supplementary Fig. S3), which is reflected by a shorter rise time in the UCNPs[33]. Therefore, there is a significant increase in the excitation efficiency resulting in enhanced upconversion luminescence[48]. Meanwhile, the decrease in decay time from τ = 186.9 μs (black curve in Fig. 5b) to τ = 141.3 μs (red curve in Fig. 5b) is also observed, which could be attributed to an increase in the radiative rate in Er^{3+} emitters within UCNPs having an optimum distance of 8 nm from the AuNRs-980 plasmon nanostructure[34]. The lifetime as a function of the thickness of polyelectrolyte multilayers and AuNRs longitudinal LSPR wavelength are shown in Fig. 5c, d. As the thickness of the polyelectrolyte multilayers increases, the upconversion luminescence rise and decay time decrease, reaching a minimum at a distance of 8 nm (Fig. 5c), corresponding to the maximum luminescence intensity (Fig. 3e). A further increase in the thickness results in increased rise and decay time. To show the effect of AuNRs longitudinal LSPR wavelength on the intensity of upconversion luminescence, we plotted the rise time and the decay time against AuNRs with different LSPR wavelengths. The minimum rise time and decay time were observed with LSPR wavelength at 980 nm, which has a largest overlap with the excitation of UCNPs. The analysis indicates the fluorescence enhancement by AuNRs can be explained by the co-effect of the rise time and decay time resulting from local field enhancement and surface plasmon-coupled emission.

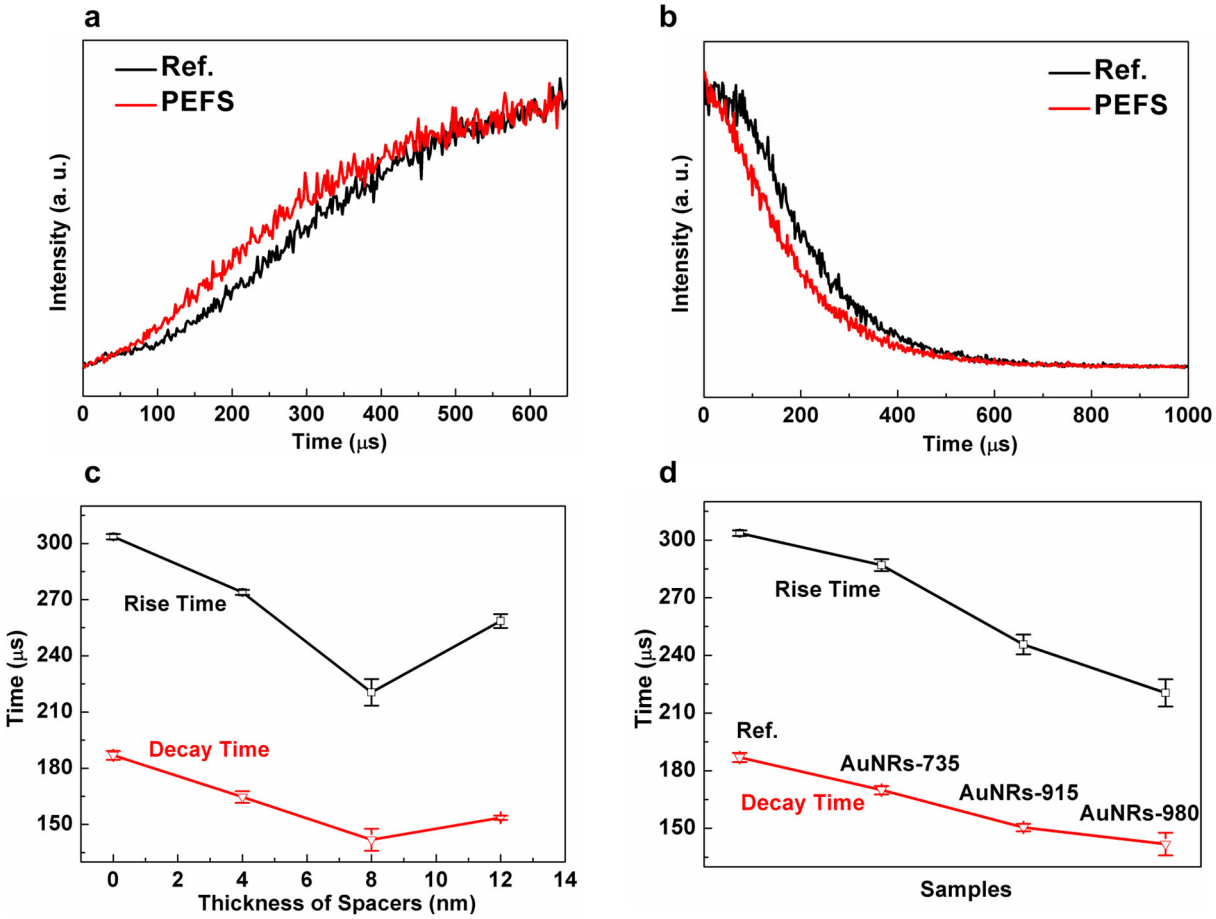

Figure 5 | Fluorescence lifetime analysis. (a) Rise time and (b) decay time curve of upconversion luminescence for UCNPs in combination with AuNRs-980 plasmon-enhancement spaced by 8 nm thickness of polyelectrolyte multilayers (PEFS, red curve) and bare UCNPs as reference (Ref., black curve). (c) Rise time (black curve) and decay time (red curve) as a function of the thickness of polyelectrolyte multilayers, which was plasmon-enhanced by AuNRs-980. (d) Rise time (black curve) and decay time (red curve) as a function of different aspect ratios of AuNRs, which was spaced by 8 nm thickness of polyelectrolyte multilayers. All the data were measured at 540 nm emission under 980 nm laser excitation. PEFS referred to UCNPs in combination with AuNRs-980 plasmon-enhancement spaced by 8 nm thickness of polyelectrolyte multilayers. And Ref. referred to barely UCNPs without AuNRs plasmon enhancement.

Analysis of penetration depth. To test the penetration capacity of plasmon-enhanced upconversion fluorescence, we performed *in vitro* upconversion fluorescence imaging using homogeneous nylon panel as tissue phantom. Nylon phantom was chosen because of its similar scattering properties as the tissues[49]. Schematic design of the setup used for UCNPs/Spacers/AuNRs imaging in tissue phantom with different thickness is shown in Fig. 6a. Upconversion luminescence graph in pseudo-color form for UCNPs enhanced by AuNRs-980 with spacer thickness of 8 nm (PEFS, top part) and bare UCNPs (Ref., bottom part) is shown in Fig. 6b. We also quantified the relationship between penetration depth (*i.e.*, phantom thickness) and fluorescence intensity (Fig. 6c). Fluorescence imaging results show that the fluorescence intensity for both PEFS and Ref. samples decreases with increasing penetration depth. The maximum penetration for UCNPs with AuNRs enhancement reaches up to 7.5 mm, while that of UCNPs without AuNRs enhancement is about 5.0 mm. The experimental results may lay the essential groundwork for exploration the applications in deeper tissue imaging of the novel ultrabright upconversion luminescence bullets.

Discussion

In comparison with other methods, fluorescence imaging by using fluorescent nanoparticles as probes is a non-destructive, high spatial resolution and high sensitivity modality for biomedical imaging[3]. Among various fluorescent nanoparticles, UCNPs are able to convert near infrared (NIR, *i.e.* 980 nm) excitation to visible emission rendering their capability for deep tissue imaging. Despite the attractive optical superiority offered by UCNPs, the development of widespread bioapplications has been limited due to low quantum yield (<1%) and the resulting low fluorescence intensity. Placing UCNPs in proximity to plasmon nanostructures can efficiently concentrate electric field into nano-volume, which has been suggested as potential means for achieving enhanced fluorescence intensity of UCNPs. However, the major challenge is to establish an effective method to study the effect of the distance and spectra properties on fluorescence properties of UCNPs in a reliable and precise manner. To meet this need, it is necessary to develop a UCNPs and AuNRs plasmon-enhanced fluorescence system by a simple and reproducible immersion-based method and evaluate the tissue penetration capacity of the system for biomedical imaging applications.

The luminescence enhancement is found to be strongly dependent upon both the thickness of the spacers and the spectra property of AuNRs. Polyelectrolyte multilayers are served as dielectric spacers to modulate the distance between UCNPs and AuNRs with nm-precision. It is demonstrated that a significant upconversion enhancement could be observed with the distance of 8 nm. By precisely tuning the LSPR wavelength of AuNRs, it is demonstrated that

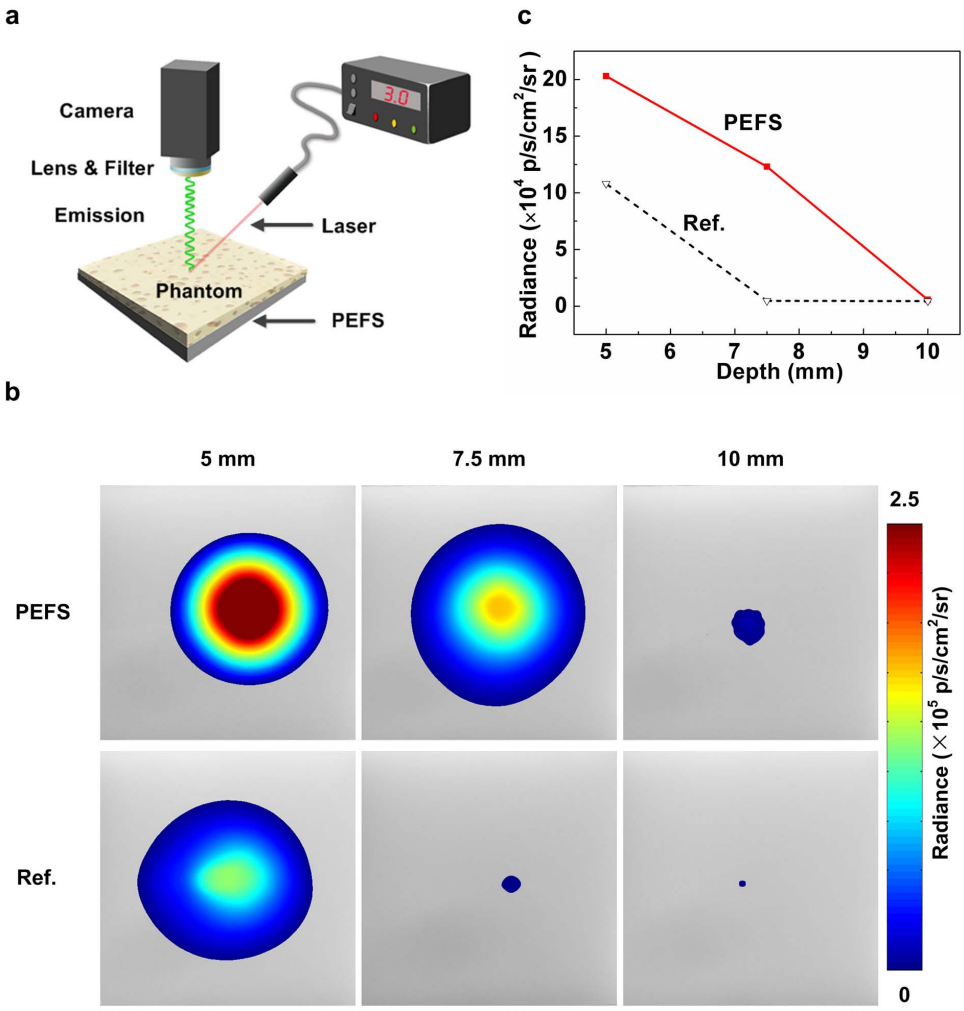

Figure 6 | Upconversion penetration assay with nylon phantoms. (a) Schematic illustration of the setup used for novel UCNPs and AuNRs plasmon-enhanced fluorescence system imaging in tissue phantom. The digital camera was used to detect the emission from the samples coved by phantoms with different thickness under the excitation of 980 nm. (b) Upconversion luminescence photos in pseudo-color form for the penetration capacity of UCNPs deposited on AuNRs-980 spaced by 8 nm thickness of polyelectrolyte multilayers (top part) and bare UCNPs (bottom part) with different thickness phantoms. (c) Quantitative analysis of the relationship between the radiance and penetration depth.

maximum overlapping of the LSPR wavelength with the excitation of UCNPs leads to most noticeable fluorescence enhancement. The experimental results are in good agreement with computational electric field simulations confirming the electric field coupling effect of AuNRs with UCNPs.

In conclusion, a maximum upconversion enhancement of up to 22.6-fold has been achieved when the thickness of spacers is 8 nm and the LSPR absorption wavelength of AuNRs overlap with excitation of UCNPs. The underlying mechanism can be explained by the combined effects of enhancement in the excitation of Yb^{3+} (sensitizer) and increase in radiative decay rate of Er^{3+} (emitter) of the UCNPs as evidenced by time-resolved upconversion luminescence measurements. Thus, the design criteria may provide a unique platform for fabrication of plasmon-enhanced upconversion nanostructures and lay the groundwork for a novel class of hybrid nanoprobes for a wide variety of biomedical imaging, biolabeling, detection and even real-time monitoring applications.

Methods

Synthesis of UCNPs and UCNPs-PAA nanoparticles. Firstly, $NaYF_4$:Yb,Er nanoparticles were prepared by thermal decomposition procedure[50]. Briefly, the rare earth chlorides including YCl_3 (0.80 mmol), $YbCl_3$ (0.18 mmol) and $ErCl_3$ (0.02 mmol) were dissolved in 2 mL distilled water by sonication to form a homogeneous solution. Then, the above solution was added to a mixed solvent of 15 mL octadecene (ODE) and 6 mL oleic acid (OA) in a 100 mL three-necked flask followed by magnetic stirring for 30 min. The slurry was heated to 150°C in a temperature-controlled electromantle to form a transparent, slightly yellow and homogeneous solution under the protection of high purified Argon gas at a rate of 10°C/min, and then cooled down to ambient temperature naturally. Next, 5 mL methanol solution with a certain amount of NaOH (2.5 mmol) and NH_4F (4 mmol) was dropped to the flask and stirred for 2 h. The mixture was then gradually heated to 100°C to remove excessive methanol and oxygen by maintained at this temperature for 30 min, and then heated to 280°C at an average rate of 20°C/min and maintained at 280°C for 1.5 h under the protection of argon. After the solution gradually cooled down, the resultant mixture was precipitated from the solution with an excess amount of ethanol, and washed with ethanol: cyclohexane (1 : 1) mixture for three times. A typical ligand-exchange process was performed by using PAA which can substitute the original hydrophobic ligands such as OA and ODE on the surface of as-prepared UCNPs. After PAA coating, the final product was stored in water at 4°C for the further use.

Preparation of CTAB-coated gold nanorods. AuNRs with different aspect ratios were synthesized by seed-mediated growth method with positive-charged hexadecyltrimethylammonium bromide (CTAB) as stabilizing agents. The seed solution was achieved by adding 0.6 mL of a 10 mmol ice-cold $NaBH_4$ solution into a 10 mL of another mixture including 0.1 M CTAB and 0.25 mmol $HAuCl_4$ aqueous solution, and stirred magnetically for 10 min. The growth solution was achieved by adding 95 mL of 0.1 M CTAB, 1.0 mL of 10 mmol $AgNO_3$, 5 mL of 10 mmol $HAuCl_4$, and 0.55 mL of 0.1 M ascorbic acid in the order. Then 0.12 mL of newly prepared seed solution was mixed with the growth solution. After a gentle mixing, the mixture was kept in dark for 16 h to obtain AuNRs with the aspect ratio of 4.5. The AuNRs with aspect ratio of 7.6 and 6.3 were purchased from Sigma Aldrich. Finally,

AuNRs were centrifuged at 10000 rpm for 15 min twice to removing the excess CTAB stabilizer and re-dispersed in distilled water.

Fabrication process of a novel UCNPs and AuNRs plasmon-enhanced fluorescence system with layer-by-layer self-assembly methods. As shown schematically in Fig. 1a, the novel UCNPs and AuNRs plasmon-enhanced fluorescence system was prepared according to the following procedure. Firstly, silicon slides were cut into rectangle shape with the size of 20 × 20 mm^2 and immersed into a piranha solution for 40 min. Then, the substrates were rinsed with DI water for three times. A positive charged AuNRs coating was attached onto pretreated negatively charged silicon substrates. Polyelectrolyte of positively charged PAH (1 mM, M_w = 15000 g/mol) and negatively charged PSS (1 mM, M_w = 13400 g/mol) were dissolved in 0.1 M sodium chloride to form a homogeneous solution. Then polyelectrolyte multilayers were assembled alternatively for 15 min using the immersion-based layer-by-layer self-assembly procedure. The process was repeated to obtain desired numbers of polyelectrolyte multilayers. Finally, following the deposition of polyelectrolyte multilayers terminated with a positively charged PAH layer, we electrostatically adsorbed the negatively charged UCNPs-PAA from an aqueous solution onto the polyelectrolyte surface. After each of the deposition steps, the substrates were washed thoroughly with distilled water and dried by N_2 atmosphere flow. In this paper, the distance-dependent plasmon-enhanced fluorescence was investigated by changing the thickness of polyelectrolyte layers as tunable spacers with AuNRs/Polyelectrolytes/UCNPs trilayer structures (Fig. 1b). And the spectra-dependent plasmon-enhanced fluorescence was also performed by changing the aspect ratio of AuNRs (Fig. 1c).

Demonstration of plasmon-enhanced fluorescence system in deep-tissue imaging. To demonstrate the penetration capacity of plasmon-enhanced fluorescence system, we performed a nylon phantom experiment. A series of thickness of the phantom including 5.0, 7.5 and 10.0 mm were chosen and then cut into the size of 20 × 20 mm^2. The digital camera (Nikon D90) was used to detect the emission from the samples coved by phantoms with different thicknesses under the excitation of 980 nm laser (Fig. 6a). The data were collected for 30 sec. The same experiment was repeated for three times.

Structural, physical and optical characterization. TEM images were taken on a JEOL JEM 2100 microscope at an accelerating voltage of 200 kV. SEM observation was performed on a JSM-6700F field emission SEM operating at 10 kV. The as-prepared UCNPs powder was characterized on an XRD-7000 diffractometer with a Cu K_α radiation. A Nano-ZS90 Zeta Sizer was used to determine zeta potentials of UCNPs and AuNRs. AFM was performed using a DI Innova AFM (Bruker) in light tapping mode. Optical absorption spectra were recorded using a UV-3600 UV-Vis-NIR absorption spectrophotometer. Upconversion fluorescent spectrum was measured via QuantaMasterTM40 spectrofluorometer equipped with a 250 mW 980 nm NIR laser diode. Fluorescence lifetime measurements were recorded on an FLsp920 spectrofluorometer (Edinburgh) with 980 nm laser light as the excitation source, which is a time-gated method compatible with the long lifetime of UCNPs. Upconversion luminescence images were achieved by a camera for 30 sec under the excitation for the tissue penetration depth test.

Finite-difference time-domain simulation. The distribution of the electric field around AuNRs was calculated by three-dimensional FDTD method with commercial software. FDTD simulations indicated spatial and temporal dependence of Maxwell's equations to model electromagnetic waves in rectangular three-dimensional cells of finite volume called Yee cells. The single AuNR with different aspect ratios was performed in a numerical domain of 300 × 300 × 200 nm^3. The absorbing boundary conditions of perfectly matched layer were obtained in different directions. Further, a higher resolution simulation was performed at a 980 nm extinction wavelength to obtain the distribution of electric field. The refractive index of AuNRs was set as n = 0.18 + 4.96 i at this frequency, and the refractive index of surrounding medium was equal to 1 as air.

1. Xie, X. & Liu, X. Photonics: Upconversion goes broadband. *Nat. Mater.* **11**, 842–843 (2012).
2. Liu, Q. *et al.* ^{18}F-Labeled magnetic-upconversion nanophosphors *via* rare-earth cation-assisted ligand assembly. *ACS Nano* **5**, 3146–3157 (2011).
3. Naczynski, D. J. *et al.* Rare-earth-doped biological composites as *in vivo* shortwave infrared reporters. *Nat. Commun.* **4**, 1–10 (2013).
4. Larson, D. R. *et al.* Water-soluble quantum dots for multiphoton fluorescence imaging *in vivo*. *Science* **300**, 1434–1436 (2003).
5. Zhou, J., Liu, Z. & Li, F. Y. Upconversion nanophosphors for small-animal imaging. *Chem. Soc. Rev.* **41**, 1323–1349 (2012).
6. Wang, F. & Liu, X. G. Recent advances in the chemistry of lanthanide-doped upconversion nanocrystals. *Chem. Soc. Rev.* **38**, 976–989 (2009).
7. Wang, F. *et al.* Simultaneous phase and size control of upconversion nanocrystals through lanthanide doping. *Nature* **463**, 1061–1065 (2010).
8. Haase, M. & Schäfer, H. Upconverting nanoparticles. *Angew. Chem. Int. Edit.* **50**, 5808–5829 (2011).
9. Lin, M. *et al.* Recent advances in synthesis and surface modification of lanthanide-doped upconversion nanoparticles for biomedical applications. *Biotechnol. Adv.* **30**, 1551–1561 (2012).
10. Idris, N. M. *et al. In vivo* photodynamic therapy using upconversion nanoparticles as remote-controlled nanotransducers. *Nat. Med.* **18**, 1580–1585 (2012).
11. Chatterjee, D. K., Gnanasammandhan, M. K. & Yong, Z. Small upconverting fluorescent nanoparticles for biomedical applications. *Small* **6**, 2781–27952795 (2010).
12. Kolesov, R. *et al.* Optical detection of a single rare-earth ion in a crystal. *Nat. Commun.* **3**, 1029 (2012).
13. Liu, Y., Tu, D., Zhu, H., Ma, E. & Chen, X. Lanthanide-doped luminescent nano-bioprobes: from fundamentals to biodetection. *Nanoscale* **5**, 1369–1384 (2013).
14. Chen, G., Ohulchanskyy, T. Y., Kumar, R., Ågren, H. & Prasad, P. N. Ultrasmall monodisperse $NaYF_4$:Yb^{3+}/Tm^{3+} nanocrystals with enhanced near-infrared to near-infrared upconversion photoluminescence. *ACS Nano* **4**, 3163–3168 (2010).
15. Huang, Q., Yu, J., Ma, E. & Lin, K. Synthesis and characterization of highly efficient near-infrared upconversion Sc^{3+}/Er^{3+}/Yb^{3+} tridoped $NaYF_4$. *J. Phys. Chem. C* **114**, 4719–4724 (2010).
16. Lin, M. *et al.* Synthesis of upconversion $NaYF_4$:Yb^{3+},Er^{3+} particles with enhanced luminescent intensity through control of morphology and phase. *J. Mater. Chem. C* **2**, 3661–3856 (2014).
17. Chen, G., Liu, H., Liang, H., Somesfalean, G. & Zhang, Z. Upconversion emission enhancement in Yb^{3+}/Er^{3+}-codoped Y_2O_3 nanocrystals by tridoping with Li^+ ions. *J. Phys. Chem. C* **112**, 12030–12036 (2008).
18. Nanting, D., Xingping, Z., Xie, L. & Xiaqin, W. Synthesis of $NaYF_4$:Yb,Er/$NaYF_4$ nanoparticles coated with PAM by *in-situ* polymerization. *J. Phys. Chem. Solids* **74**, 480–486 (2013).
19. Yi, G. S. & Chow, G. M. Water-soluble $NaYF_4$:Yb,Er(Tm)/$NaYF_4$/polymer core/shell/shell nanoparticles with significant enhancement of upconversion fluorescence. *Chem. Mater.* **19**, 341–343 (2007).
20. Wang, F. *et al.* Tuning upconversion through energy migration in core-shell nanoparticles. *Nat. Mater.* **10**, 968–973 (2011).
21. Zhang, W., Ding, F. & Chou, S. Y. Large enhancement of upconversion luminescence of $NaYF_4$:Yb^{3+}/Er^{3+} nanocrystal by 3D plasmonic nano-antennas. *Adv. Mater.* **24**, OP236–OP241 (2012).
22. Zhang, H., Xu, D., Huang, Y. & Duan, X. F. Highly spectral dependent enhancement of upconversion emission with sputtered gold island films. *Chem. Commun.* **47**, 979–981 (2011).
23. Zhang, F. *et al.* Fabrication of Ag@SiO_2@Y_2O_3:Er nanostructures for bioimaging: tuning of the upconversion fluorescence with silver nanoparticles. *J. Am. Chem. Soc.* **132**, 2850–2851 (2010).
24. Schietinger, S., Aichele, T., Wang, H. Q., Nann, T. & Benson, O. Plasmon-enhanced upconversion in single $NaYF_4$:Yb^{3+}/Er^{3+} codoped nanocrystals. *Nano Lett.* **10**, 134–138 (2010).
25. Zhang, H. *et al.* Plasmonic modulation of the upconversion fluorescence in $NaYF_4$:Yb/Tm hexaplate nanocrystals using gold nanoparticles or nanoshells. *Angew. Chem. Int. Edit.* **49**, 2865–2868 (2010).
26. Chen, G., Qiu, H., Prasad, P. N. & Chen, X. Upconversion nanoparticles: design, nanochemistry, and applications in theranostics. *Chem. Rev.* **114**, 5161–5124 (2014).
27. Reineck, P. *et al.* Distance and wavelength dependent quenching of molecular fluorescence by Au@SiO_2 core-shell nanoparticles. *ACS nano* **7**, 6636–6648 (2013).
28. Song, J. H., Atay, T., Shi, S., Urabe, H. & Nurmikko, A. V. Large enhancement of fluorescence efficiency from CdSe/ZnS quantum dots induced by resonant coupling to spatially controlled surface plasmons. *Nano Lett.* **5**, 1557–1561 (2005).
29. Willets, K. A. & Van Duyne, R. P. Localized surface plasmon resonance spectroscopy and sensing. *Annu. Rev. Phys. Chem.* **58**, 267–297 (2007).
30. Zhang, X. *et al.* Experimental and theoretical investigation of the distance dependence of localized surface plasmon coupled förster resonance energy transfer. *ACS Nano* **8**, 1273–1283 (2014).
31. Yuan, P. *et al.* Plasmon enhanced upconversion luminescence of $NaYF_4$:Yb,Er@SiO_2@Ag core-shell nanocomposites for cell imaging. *Nanoscale* **4**, 5132–5137 (2012).
32. Luo, Q. *et al.* Large enhancements of $NaYF_4$:Yb/Er/Gd nanorod upconversion emissions via coupling with localized surface plasmon of Au film. *Nanotechnology* **25**, 185401 (2014).
33. Saboktakin, M. *et al.* Metal-enhanced upconversion luminescence tunable through metal nanoparticle-nanophosphor separation. *ACS nano* **6**, 8758–8766 (2012).
34. Saboktakin, M. *et al.* Plasmonic enhancement of nanophosphor upconversion luminescence in Au nanohole arrays. *ACS nano* **7**, 7186–7192 (2013).
35. Xu, W. *et al.* Ultra-broad plasma resonance enhanced multicolor emissions in an assembled Ag/$NaYF_4$:Yb,Er nano-film. *Nanoscale* **4**, 6971–6973 (2012).
36. Ye, X. *et al.* Morphologically controlled synthesis of colloidal upconversion nanophosphors and their shape-directed self-assembly. *Proc. Natl. Acad. Sci.* **107**, 22430–22435 (2010).
37. Wu, S. *et al.* A highly sensitive fluorescence resonance energy transfer aptasensor for staphylococcal enterotoxin B detection based on exonuclease-catalyzed target recycling strategy. *Anal. Chim. Acta.* **782**, 59–66 (2013).
38. Gandra, N. *et al.* Probing distance-dependent plasmon-enhanced near-infrared fluorescence using polyelectrolyte multilayers as dielectric spacers. *Angew. Chem.* **125**, 1–6 (2013).

39. Priyam, A., Idris, N. M. & Zhang, Y. Gold nanoshell coated $NaYF_4$ nanoparticles for simultaneously enhanced upconversion fluorescence and darkfield imaging. *J. Mater. Chem.* **22**, 960–965 (2012).
40. Paudel, H. P. *et al*. Enhancement of near-infrared-to-visible upconversion luminescence using engineered plasmonic gold surfaces. *J. Phys. Chem. C* **115**, 19028–19036 (2011).
41. Ge, W. *et al*. Distance dependence of gold-enhanced upconversion luminescence in $Au/SiO_2/Y_2O_3$: Yb^{3+}, Er^{3+} nanoparticles. *Theranostics* **3**, 282 (2013).
42. Shen, J. *et al*. Influence of SiO_2 layer thickness on plasmon enhanced upconversion in hybrid $Ag/SiO_2/NaYF_4$:Yb,Er,Gd structures. *Appl. Sur. Sci.* **270**, 712–717 (2013).
43. Kang, K. A., Wang, J., Jasinski, J. B. & Achilefu, S. Fluorescence manipulation by gold nanoparticles: from complete quenching to extensive enhancement. *J. Nanobiotechnol.* **9**, 16 (2011).
44. Lakowicz, J. R. Radiative decay engineering: biophysical and biomedical applications. *Anal. Biochem.* **298**, 1–24 (2001).
45. Lakowicz, J. R. Radiative decay engineering 5: metal-enhanced fluorescence and plasmon emission. *Anal. Biochem.* **337**, 171–194 (2005).
46. Bharadwaj, P. & Novotny, L. Spectral dependence of single molecule fluorescence enhancement. *Opt. Express* **15**, 14266–14274 (2007).
47. Chen, C. D., Cheng, S. F., Chau, L. K. & Wang, C. R. C. Sensing capability of the localized surface plasmon resonance of gold nanorods. *Biosens. Bioelectron.* **22**, 926–932 (2007).
48. Tam, F., Goodrich, G. P., Johnson, B. R. & Halas, N. J. Plasmonic enhancement of molecular fluorescence. *Nano Lett.* **7**, 496–501 (2007).
49. Ma, X. *et al*. Enhancement of Cerenkov luminescence imaging by dual excitation of Er^{3+}, Yb^{3+}-doped rare-earth microparticles. *PLOS ONE* **8**, e77926 (2013).
50. Fan, W. *et al*. Rattle-structured multifunctional nanotheranostics for synergetic chemo-/radiotherapy and simultaneous magnetic/luminescent dual-modal imaging. *J. Am. Chem. Soc.* **135**, 6494–6503 (2013).

Acknowledgments

This work was financially supported by the National Natural Science Foundation of China (11120101002), International Science & Technology Cooperation Program of China (2013DFG02930), National Key Scientific Apparatus Development of Special Item (2013YQ190467), Natural Science Basic Research Plan in Shaanxi Province of China (2014JQ6199), the Fundamental Research Funds for the Central Universities (2012jdhz46). M.L. is supported by scholarship from the China Scholarship of Council. Feng Xu was also partially supported by the China Young 1000-Talent Program and the Program for New Century Excellent Talents in University. The SEM and TEM work was done at International Center for Dielectric Research (ICDR), Xi'an Jiaotong University, Xi'an, China. The authors also thank Ms. Dai Yan Zhu, Ms. Lu Lu and Mr. Ma Chuan Sheng for their help in using SEM and TEM.

Author contributions

M.L., F.X. and S.S. conceived the study and designed the experiment. A.L.F., M.L.Y. and M.L. performed the experiment. L.M.T. and S.S. performed the AuNRs synthesis and the simulation. M.L., F.X., T.J.L. Z.F.D. and A.L.F. performed the data analysis. M.L., F.X., T.J.L. Z.F.D. and A.L.F. wrote the manuscript. All authors contributed to the interpretation and discussion of the results.

Additional information

Supplementary information accompanies this paper at http://www.nature.com/scientificreports

Competing financial interests: The authors declare no competing financial interests.

How to cite this article: Feng, A.L. *et al*. Distance-Dependent Plasmon-Enhanced Fluorescence of Upconversion Nanoparticles using Polyelectrolyte Multilayers as Tunable Spacers. *Sci. Rep.* **5**, 7779; DOI:10.1038/srep07779 (2015).